NMR of Inorganic Solids

Eric Oldfield
University of Illinois at Urbana-Champaign, Urbana, IL, USA

Abbreviations

CP-MAS = cross polarization magic angle sample spinning; CSA = chemical shift anisotropy; DAS = dynamic angle sample spinning; DOR = double rotation; MAS = magic angle sample spinning; VAS = variable angle sample spinning.

1 INTRODUCTION

While NMR spectra of many inorganic solids (metals, alloys, single crystal minerals, etc.) have been reported since the earliest days of NMR, only at the beginning of the 1980s did solid state NMR begin to find widespread applications in inorganic chemistry, the materials sciences, and geochemistry.[1] The main reason for this delay is simple: almost no one tried to get high-resolution spectra from inorganic solids! An exception to this is the work of E. R. Andrew.[2-4] He obtained 'high-resolution' spectra of ^{23}Na in NaCl (an easy system since it is cubic and has no quadrupolar broadening) but he also made the important NMR observation that solid PCl_5 exists as $[PCl_4]^+[PCl_6]^-$,[3] discovering at the same time the rotational resonance phenomenon.[3] His group also observed that the Knight shift anisotropy of Cd broke up into numerous spinning sidebands on slow magic angle sample spinning (MAS),[4] a basic phenomenon rediscovered much later in the ^{13}C and ^{29}Si arena. The rapid increase in availability of high-field (≥200 MHz ^{1}H resonance frequency) multinuclear instruments which began around 1980 soon led numerous groups to explore the feasibility of analyzing inorganic solids by MAS NMR, and the area began to blossom, with extensive investigations of ^{23}Na, ^{27}Al, and ^{29}Si being reported.[5-8] In what follows, we will first describe solid state NMR applications to quadrupolar nuclei, and then follow this by a discussion of spin $I = \frac{1}{2}$ systems. *Quadrupolar* nuclei are by far the most abundant spin systems in the Periodic Table but they are more difficult to observe than $I = \frac{1}{2}$ systems. We therefore use a technique-oriented approach for the quadrupoles, while for the spin $-\frac{1}{2}$ systems we use a nucleus-by-nucleus approach, since the observational technique is invariably MAS or a simple variant thereof.

2 SOLID STATE NMR OF QUADRUPOLAR NUCLEI

2.1 MAS NMR

As early as 1959, Andrew reported the observation of significant line narrowing on rapidly rotating a sample at the 'magic angle' of 54.7° to the main magnetic field B_0.[2] He used NaCl, which is cubic, and was mainly interested in removing the strong dipole–dipole interactions between ^{23}Na spins, but surprisingly, with the exception of some studies of cubic ^{27}AlP and ^{133}CsCl, there was little follow up to his work. In retrospect, the whole area of ^{27}Al, ^{29}Si MAS NMR could have blossomed in the late 1960s, but it did not. However, with the increasing availability of high-field MAS NMR instrumentation, many workers began to reinvestigate ^{23}Na[9] and ^{27}Al,[6,7] as well as ^{11}B[10] and more exotic species such as ^{93}Nb,[11] and the inorganic solids era had arrived.

In early work, Lippmaa et al.[8] made the important observation that the central $\frac{1}{2} \leftrightarrow -\frac{1}{2}$ spin transition of ^{23}Na in the noncubic material $NaNO_2$ could be readily observed by using straightforward MAS NMR techniques, and a lineshape analysis permitted the determination of the isotropic chemical shift, δ_{iso}, the nuclear quadrupole coupling constant, e^2qQ/h, and the asymmetry parameter of the electric field gradient, η, given by equation 1:

$$\eta = \frac{|V_{xx} - V_{yy}|}{V_{zz}} \quad (1)$$

although accurate ab initio computation of these parameters (see *Ab Initio Calculations*) in most systems is still lacking. For example, the chemical shift of ^{23}Na in solid NaCl has been known for 35 years, but has not yet been rigorously computed. Notwithstanding this, MAS NMR has proven to be an exceptionally important technique with which to probe the structures of inorganic solids. Excellent books on silicates and zeolites are available,[12,13] and by way of example we show in Table 1 a compilation of e^2qQ/h, η, and δ_{iso} values for ^{27}Al in a collection of common aluminosilicate minerals and synthetic zeolites.[13] For ^{27}Al the single most useful spectral parameter is δ_{iso}, which for Al in octahedral coordination (see *Octahedral*) in aluminas and aluminosilicates resonates around 0–10 ppm,

For References see p.2658

while for Al in tetrahedral coordination (see *Tetrahedral*) $\delta_{iso} \approx$ 55–80 ppm.[12,13] More exotic species, such as pentahedral Al, have been proposed to resonate at around 30 ppm.[13] Thus, a simple MAS NMR experiment gives information on coordination number (see ***Coordination Numbers & Geometries***). In the case of aluminosilicates, this can be a useful monitor of framework (tetrahedral) or nonframework (octahedral) location, although determination of other spectral parameters is often necessary for confirmation of such an assignment.

Table 1 Nuclear Quadrupole Coupling Constants, Electric Field Gradient Tensor Asymmetry Parameters, and Isotropic Chemical Shifts of ^{27}Al in Aluminosilicates[13]

Aluminosilicate	e^2qQ/h (MHz)	η	δ_{iso} (ppm)
Sillimanite	6.77	0.532	64.5
	8.93	0.462	4.0
Andalusite	5.9	0.69	36.0
	15.7	0.08	–
Kyanite	6.53	0.59	7.5
	3.70	0.89	5.0
	9.37	0.38	–
	10.04	0.27	–
Penninite	2.8	–	72
	1.4	–	10
Muscovite	2.1	–	72
	2.2	–	5
Margarite	4.2	0.5	76
	6.3	0.1	11
Xanthophyllite	2.8	–	76
	2.0	–	11
Albite	3.29	0.62	62.7
Microcline	3.22	0.21	58.5
Natrolite	1.67	0.503	64.0
Zeolite NaA	1.1	0.75	59.2
Zeolite NaY	2.0	0.5	62.8

2.2 Second-Order Effects

An unusual effect found with NMR of quadrupolar nuclei in many materials is that the observed chemical shift is not the isotropic chemical shift. The reason for this is that there is a so-called second-order shift of the resonance line[13] due to perturbation of the Zeeman levels by the quadrupolar interaction. The effect scales in ppm as $(e^2qQ/h)^2/\nu_L^2$, where ν_L is the Larmor frequency, the quadrupolar shift, σ_{qs}, being given by equation 2:

$$\sigma_{qs} = \delta_{cg} - \delta_{iso} = -\frac{4}{15} \times 10^6 \left(1 + \frac{\eta^2}{3}\right) \frac{\nu_Q^2}{\nu_L^2} \qquad (2)$$

where δ_{cg} is the center of gravity of the (static or MAS) lineshape, and ν_Q for ^{27}Al = $(3/20)(e^2qQ/h)$. If ν_Q and η are known, equation 2 permits a good estimate of δ_{iso}, and if field dependence studies are carried out (varying ν_L), then graphical methods can be used to obtain even more precise values. If ν_Q and η are unknown, then σ_{qs} and ν_Q can still be estimated quite reliably, since the $\eta^2/3$ term contributes at most a 15% error.

2.3 Variable Angle Sample Spinning

Since the quadrupolar interaction to second order does not transform like a second-rank tensor ($P_2(\cos\theta)$), then optimum angles for line narrowing other than $\theta = 54.7°$ ($P_2(\cos\theta) = 0$) are expected. In early work, Nolle[14] found that spinning a $Mo(CO)_6$ sample at 90° to B_0 gave an unusual ^{95}Mo NMR lineshape, due to averaging of the second-order ^{95}Mo quadrupole interaction,[14] and this so-called 'variable angle' sample spinning (VAS) approach was soon extended to ^{11}B in borosilicates[10] and ^{23}Na in Na_2MoO_4 and Na_2SO_4.[9] Figure 1 shows an example in which ^{11}B NMR is observed in a borosilicate glass, for a static sample, and spinning at 54.7°, 36°, and 75°.[10] The 75° VAS NMR spectrum has considerably better resolution, due to more effective averaging of the second-order quadrupolar interaction of the trigonal (BO_3) sites. However, complete averaging requires spinning about two axes, to average both first- and second-order interactions, as described in Section 2.4.

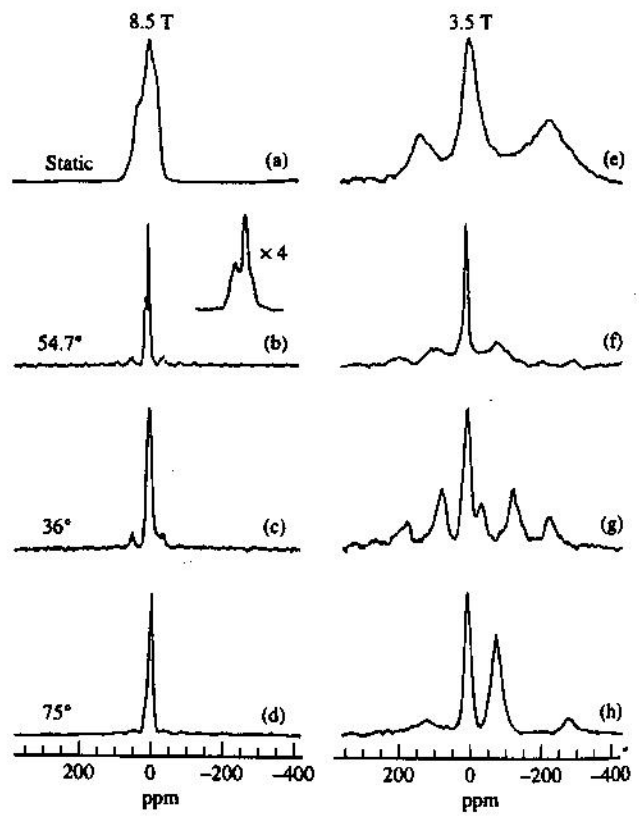

Figure 1 Boron-11 NMR spectra of a borosilicate glass at 8.45 and 3.52 T. (a)–(d), 8.45 T static, MAS, and VAS (36°, 75°) spectra; (e)–(h), 3.52 T static, MAS, and VAS (36°, 75°) spectra. (Reproduced by permission of the Royal Society of Chemistry from Schramm and Oldfield[10])

List of General Abbreviations on back endpaper

2.4 Spinning Around Two Axes

The MAS and VAS techniques described above can give factors of ~3.6 up to ~10 decreases in linewidth, with residual second-order quadrupolar broadening preventing further decreases. Two ways around this limitation have been found, in which samples experience rotation at two different angles, thereby averaging both first- and second-order quadrupolar interactions. The origins of these experiments can be understood as follows: for a first-order quadrupolar interaction the broadening is described by a second-rank tensor, $P_2(\cos\beta)$, and averages to zero under MAS, where $\beta = \arccos(1/\sqrt{3}) = 54.7°$. However, for second-order broadening, when ν_Q is a significant fraction of ν_L, there is a further broadening, described by the second-order quadrupolar frequency shift (equation 3):

$$\upsilon - \upsilon_L = \upsilon_{cg} + \sum_{i=2,4} A_i(\phi,\psi) P_i(\cos\beta) \qquad (3)$$

where ν_{cg} is the center of gravity of the line, $A_i(\phi,\psi)$ are Euler angle dependent terms describing transformations between the quadrupole principal axis system and the rotor axis, and $P_i(\cos\beta)$ are terms which depend on the rotor axis orientations (β) in B_0, and are given by equation 4:

$$P_2(\cos\beta) = \frac{1}{2}(3\cos^2\beta - 1); \quad P_4 = \frac{1}{8}(35\cos^4\beta - 30\cos^2\beta + 3) \qquad (4)$$

The first term is zero when $\beta = 54.7°$, the magic angle. The second term is zero when $\beta = 30.55°$ or $70.12°$, close to the optimum VAS angles.[15] Thus to obtain maximum line narrowing of a second-order quadrupolar lineshape, spins need to experience the effects of both P_2 and P_4 averaging. Conceptually, if not experimentally, the most straightforward way to achieve simultaneous rotation at two angles is to have a rotor within a rotor, a challenge successfully met by Samoson, Lippmaa, and Pines[16] in their double rotation or DOR technique. Here, an outer MAS rotor, typically ~20 mm o.d., contains a much smaller inner rotor, having an angle between rotation axes of ~30.6°. The inner rotor spins about five times faster than the outer, with maximum rates of ~0.8, 4.0 kHz being obtainable. The DOR method gives exceptionally good resolution, but it has low sensitivity since most of the receiver coil is empty.

The second approach to rotation about multiple axes is the so-called dynamic angle spinning or DAS technique.[17,18] Here, the sample is toggled between two or even three axes, and either one- or two-dimensional spectra can be obtained. The technique is simpler to implement than DOR, has better sensitivity, and has been used to determine δ_{iso}, e^2qQ/h, and η information for ^{17}O nuclei in silicates[19,20] and silicate glasses,[21] as well as in, for example, a series of Rb salts.[22] Figure 2 shows 11.7 T ^{87}Rb DAS NMR results on $RbNO_3$. There are three Rb sites, characterized by $\delta_{iso} = -26.2$, -26.8, and -30.9 ppm, having e^2qQ/h, η values of 1.83 MHz, 0.12; 2.07 MHz, 1.00; and 1.85 MHz, 0.48. Determination of e^2qQ/h, η, and δ_{iso} requires either a computer lineshape analysis or a field dependence study;[22] for example, the ~0 and ~1 asymmetry parameters for sites a,b are clearly visible from the powder pattern cross sections shown in Figure 2.[22] The DAS method requires T_1 values longer than the time required to flip the axis, and relatively weak dipolar interactions during flipping. For systems such as oxidic glasses both criteria are usually met, and the 2D DAS method appears to have considerable utility for deconvoluting quadrupole and chemical shift information in these and related materials.[21]

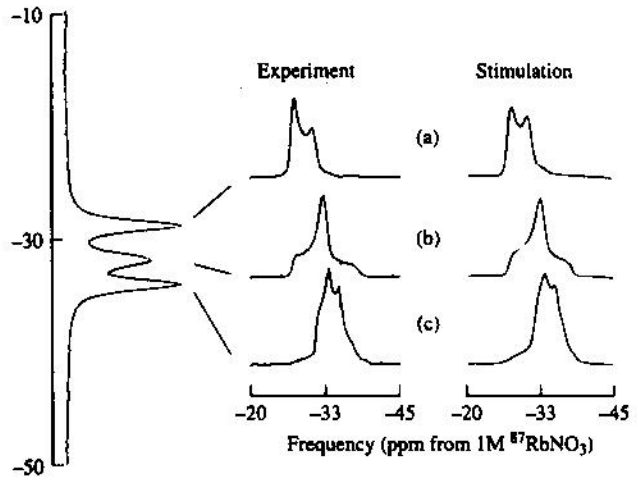

Figure 2 Rubidium-87 NMR spectra of $RbNO_3$ at 11.7 Tesla showing isotropic peaks (at –29, –32, and –34 ppm), correlated with second-order powder patterns by means of pure phase DAS. (Reproduced by permission of the American Chemical Society from Baltisberger et al.[22])

2.5 Oxygen-17 NMR

Oxygen-17 is the only stable isotope of oxygen which has a nuclear spin, $I = \frac{5}{2}$ (and a quadrupole moment of -2.610×10^{-2} barns). It is of particular interest in inorganic chemistry and geochemistry since oxygen is the most abundant element in the Earth's crust, as well as being a major constituent of many other materials, ranging from zeolites and high T_c superconductors to organometallics and even to proteins. Although this isotope has only a very low natural abundance (0.037%), ^{16}O can often be readily exchanged for ^{17}O by gas phase or hydrothermal methods; alternatively, ^{17}O-labeled ligands (such as CO or O_2) can be directly incorporated into the system of interest. The earliest studies of ^{17}O labeled compounds involved labeling of simple binary oxides such as MgO, Al_2O_3, and SiO_2,[23] as well as more complex silicates, such as forsterite (Mg_2SiO_4) and diopside ($CaMgSi_2O_6$).[23,24] Using MAS it is possible to determine the isotropic chemical shifts for ^{17}O, as well as e^2qQ/h and η values for individual sites. For example, as shown in Figure 3, diopside yields a broad, relatively featureless line when static, but under MAS (or VAS) the $\frac{1}{2}$, $-\frac{1}{2}$ transitions of the bridging and nonbridging sites are largely resolved (Figure 3d), and the δ_{iso}, e^2qQ/h, and η parameters can be extracted via lineshape simulation (Figure 3e).[25] Diopside is a chain silicate, in which the chains of silicate tetrahedra are parallel to one of

For References see p.2658

the crystallographic axes, and the chains can be visualized as being held together by the divalent cations. Within each chain, each [SiO_4] tetrahedron shares two oxygens with adjacent tetrahedra (bridging oxygens, Si–O–Si), and also contains two crystallographically nonequivalent oxygens which are coordinated to the divalent cations (nonbridging oxygens, Si–O–M). The bridging oxygens are also coordinated to either one or two divalent cations. Three crystallographically distinct oxygen sites thus exist, two nonbridging and one bridging. For the two nonbridging sites in diopside, e^2qQ/h = 2.7 MHz, η = 0, and δ_{iso} = 84, 63 ppm, while for the single oxygen bridging the two SiO_4 tetrahedra, e^2qQ/h = 4.4 MHz, η = 0.3, and σ_i = 69 ppm.[25] Upon substitution of the Ca, Mg cations by other Group 2 cations there are significant changes in δ_{iso} and e^2qQ/h (Table 2). There are large deshieldings observed for the nonbridging oxygens as the radius of the alkaline earth cation increases, while the bridging oxygen is relatively unaffected. Good empirical correlations between cation radius and chemical shift have been reported, so that ^{17}O NMR is a potentially powerful technique with which to probe the structures of complex oxides. Even more complex (sheet) silicates, such as talc ($Mg_3Si_4O_{10}(OH)_2$),[26] tectosilicates such as Linde A and Y zeolites, and aluminophosphates such as the porous $AlPO_{4-n}$ materials, have now been investigated by using ^{17}O NMR, and many structural correlations have been noted.[27]

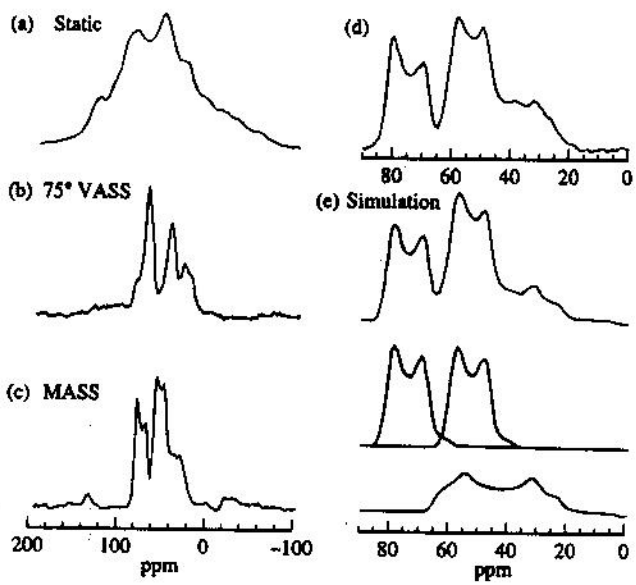

Figure 3 Oxygen-17 NMR spectra and spectral simulations of crystalline diopside ($CaMgSi_2O_6$) at 11.7 T: (a) static; (b) 75° VAS; (c) MAS; (d) expansion of center band of (c); (e) simulation of (d) with individual spectral components, two nonbridging oxygens, and one bridging oxygen. (Reproduced by permission of the American Chemical Society from Timken et al.[25])

In Linde A and Linde Y zeolites, the effects of Si, Al on ^{17}O e^2qQ/h and δ_{iso} values can be clearly seen.[27] In Linde Y there are two types of oxygen: SiOSi and SiOAl, characterized by e^2qQ/h values of ~5.0 and 3.2 MHz, respectively. These values

Table 2 Oxygen-17 Nuclear Quadrupole Coupling Constants, Asymmetry Parameters, and Isotropic Chemical Shifts for the Alkaline Earth Metasilicates[a]

System	Oxygen type	e^2qQ/h (MHz)	η	δ_{iso} (ppm)
$MgSiO_3$	O_{nb}	3.2	0.0	60
	O_{nb}	3.2	0.0	42
	O_{br}	5.1	0.3	62
$CaMgSi_2O_6$	O_{nb}	2.8	0.0	85
	O_{nb}	2.8	0.1	64
	O_{br}	4.5	0.3	70
α-$CaSiO_3$	O_{nb}	2.1	0.1	94
	O_{nb}	2.3	0.1	91
	O_{br}	3.8	0.2	75
α-$SrSiO_3$	O_{nb}	2.1	0.1	108
	O_{nb}	2.2	0.1	105
	O_{br}	4.1	0.4	80
$BaSiO_3$	O_{nb}	2.1	0.1	169
	O_{nb}	1.6	0.1	159
	O_{br}	3.7	0.4	87

[a]Adapted from Timken et al.[25]

are extremely similar to those found in pure *Silica* (low cristobalite, e^2qQ/h = 5.3 MHz), which has solely SiOSi bonds, or the zeolite Linde A (e^2qQ/h = 3.2 MHz), indicating very similar local bonding around oxygen, and the ^{17}O NMR spectrum of Linde Y can be approximated as the sum of the spectra of SiO_2 plus Linde A (SiOAl sites). Dealumination of Linde Y produces SiO_2 polymorphs (see *Polymorph*) having e^2qQ/h = 5.2 MHz, close to that found in pure silica. Since the two ^{17}O sites in Linde A can be differentiated on the basis of e^2qQ/h and δ_{iso}, it is possible to determine the Si:Al ratio (as with ^{29}Si NMR, see Section 3.1), with in this case the Si:Al ratio being given by equation 5:

$$\frac{Si}{Al} = \frac{2\left(\frac{1}{4}I_1\right) + \frac{1}{4}I_2}{\frac{1}{4}I_2} \qquad (5)$$

where I_1 is the percentage of SiOSi sites, and I_2 the percentage of SiOAl sites ($I_1 + I_2 = 100$). In SiO_2, Linde A, and Linde Y there are small differences in apparent e^2qQ/h values obtained from static and MAS NMR spectra, an effect thought to be due to a small ^{17}O chemical shift anisotropy. For $AlPO_{4-n}$ materials, ^{17}O NMR shows decreased shielding (to ~62 ppm) and an increase in e^2qQ/h (to ~5.6 MHz), generally attributable to an increase in covalent bonding (see *Covalent Bonds*).

The chemical shifts of many binary oxides have also been reported,[28] and empirical correlations with, for example, cation radius have been made, although full ab initio shielding calculations have not been reported. For some binary oxides, such as many lanthanide oxides, the observed chemical shift range is exceedingly large (Gd_2O_3 ~ −11 000 ppm; Nd_2O_3 ~3000 ppm) due to the presence of paramagnetic cations:[28] the observed shift is found to be proportional to $\langle S_Z \rangle$, the averaged spin moment, and hyperfine fields can be estimated.

List of General Abbreviations on back endpaper

^{17}O NMR shieldings in other complex oxides and oxoanions (see *Oxoanion*), such as MnO_4^-, WO_4^{2-}, and $V_{10}O_{28}^{6-}$, have been reported[24] and show unusual behavior. For example, ^{17}O MAS NMR spectra of MnO_4^- and WO_4^{2-} show considerable differences. In MnO_4^{2-} there is a single resonance at $\delta_{iso} = 1197$ ppm, having a width of 400 Hz (~6 ppm). The lack of any appreciable spinning sidebands indicates $e^2qQ/h \approx 0$, and the presence of only a single line indicates the presence of four magnetically equivalent oxygens, consistent with the X-ray structure of $KMnO_4$. In contrast, the MAS NMR spectrum of $K_2W^{17}O_4$ contains 10 groups of three lines! The frequency separations between the 10 groups correspond to the spinning frequency and change with spinning rate, while the separations between the three peaks remain constant.[24] Thus these peaks represent the three nonequivalent oxygens in the WO_4^{2-} ion, in accord with peak intensity measurements. For K_2WO_4 the isotropic ^{17}O chemical shifts are 437, 429, and 422 ± 1 ppm from external $H_2{}^{17}O$, and an analysis of the sideband intensity ratios as a function of spinning speed according to the method of Herzfeld and Berger[29] yields the following chemical shift tensors: $\sigma_{11}{}^1 = 564$, $\sigma_{22}{}^1 = 530$, and $\sigma_{33}{}^1 = 217$ ppm; $\sigma_{11}{}^2 = 567$, $\sigma_{22}{}^2 = 518$, and $\sigma_{33}{}^2 = 202$ ppm; $\sigma_{11}{}^3 = 561$, $\sigma_{22}{}^3 = 497$, and $\sigma_{33}{}^3 = 208$ ppm, where the values for σ^1 represent the shift tensor for the two equivalent oxygens in the WO_4^{2-} ion. As with the binary oxides, it seems reasonable to expect a correlation between cation ionic radius and oxygen-17 chemical shift in a series of isoelectronic structures, and results for a series of Group 5–10 oxides and oxoanions show that this is the case.[24] Solid state ^{17}O NMR has also been applied to investigating much more complex species, such as the basic zinc dithiophosphate (μ_4-[^{17}O]-oxo)hexakis(μ-*O,O*-diisopropylphosphorodithioato)tetrazinc, as well as cesium decavanadate ($Cs_6V_{10}{}^{17}O_{28}$), a polyoxoanion related to the naturally occurring mineral pascoite ($Ca_3V_{10}O_{28}\cdot 17H_2O$), where large CSA interactions are seen.[24] Large CSA interactions have also been observed when oxygen is involved in multiple bonding to lighter elements, although often the CSA interaction is masked by second-order quadrupolar effects (e.g. in ketone groups[30]). However, in carbon monoxide[30] ligands, e^2qQ/h values are typically only ~1 MHz, and in e.g. the Cr, Mo, and W hexacarbonyls, CSA values of 691, 650, and 619 ppm have been reported.[31] Upon displacement of CO ligands, to form e.g. Mo(bipy)$(CO)_4$, *cis* and *trans* carbonyl groups can be resolved, making ^{17}O MAS NMR a potentially useful complement to the more conventional ^{13}C NMR method for investigating the structures of ***Carbonyl Complexes of the Transition Metals***.[31]

When both quadrupolar and chemical shift anisotropy interactions cause line broadening, single crystal studies may be required in order to determine e^2qQ/h, η, and the components of the chemical shielding tensor. In other cases, computer lineshape analyses[32,33] may be used to help deconvolute spectra. Analysis of powder pattern lineshapes of $^{17}O_2$ ligands (see ***Dioxygen & Related Ligands***) bound to heme protein models (see *Heme Proteins*) such as picket fence *Porphyrin*,[34] as well as myoglobin and hemoglobin themselves, have been reported[34] and show exceptionally large CSA values. In the picket fence porphyrin–$^{17}O_2$ adduct, at 298 K, $\sigma_{11}{}^a = 1600$, $\sigma_{22}{}^a = 1600$, $\sigma_{33}{}^a = 2850$; $\sigma_{11}{}^b = 0$, $\sigma_{22}{}^b = 2150$, $\sigma_{33}{}^b = 2650$ ppm have been measured, where a = the terminal and b = the bridging oxygen. These unprecedented CSA values presumably arise due to the proximity of nearby excited states (see *Excited State*).[34] The ^{17}O chemical shifts in the heme proteins and picket fence systems are similar to those found in O_3, and give some support for ozone-like contributions to bonding in the Fe–O–O fragment.[34]

2.6 Boron-11 NMR

Boron-11 has $I = \frac{3}{2}$, $eQ = 0.04$ barns, and a natural abundance of 80.22%; because of its high abundance, sensitivity, and relatively small quadrupole moment, it has been extensively studied in inorganic solids (see ***Borates: Solid State Chemistry***). In pioneering work, Bray et al.[35] used continuous wave wide-line NMR methods to investigate the structures of many alkali borate glasses. There are two main classes of boron site: trigonal (BO_3) and tetrahedral (BO_4), which resonate at ~20 and ~0 ppm from an external standard of $BF_3\cdot Et_2O$. Wide-line methods give a good account of the relative amounts of trigonal and tetrahedral boron, and also permit a determination of the fraction of BO_3 units having all bridging, or one or more nonbridging, oxygens.[35] In the alkali borosilicate system Na_2O–B_2O_3–SiO_2 (see *Borosilicate Glass*), Yun and Bray have shown that for a sodium oxide to boron oxide ratio of 0.5 or less, the sodium ions are attracted primarily by the borate network; therefore the ternary glasses can be viewed as binary sodium borate glasses diluted by SiO_2.[35] When the sodium oxide to boron oxide ratio exceeds 0.5, the additional Na_2O results in the formation of reedmergnerite $[BSi_4O_{10}]^-$ units at the expense of diborate and SiO_4 units. In this process, sodium ions are taken up only by the borate network. After all the available SiO_4 units are consumed (to form $BSi_4O_{10}^-$), additional Na^+ are proportionally shared between the borate and silicate networks. Bray et al. also pioneered the use of ^{10}B NMR ($I = 1$, $eQ = 0.08$ barns), and found ^{10}B to be in some cases even more sensitive to structural details,[36] permitting quantitative determination in glasses of many structural groupings found in crystalline compounds of the glass forming systems. Results on Li, Na, K, Rb, and Cs borate glasses at various alkali contents showed a strong dependence of the fraction of tetrahedral sites on the alkali cation,[37] and results on half and half mixed (Li–Na, Li–K, Li–Rb, Li–Cs) borate glasses at different total alkali contents have supported the mixed alkali pairing model suggested previously.[36,37]

As well as wide-line studies, many workers have used high-field ^{11}B MAS NMR to investigate borates and borosilicate materials. For borates containing H_2O or OH groups, best spectral resolution is obtained by using ^1H decoupling to remove ^{11}B–^1H dipolar interactions. In borosilicates and borosilicate glasses, this is usually unnecessary. In crystalline zeolites containing framework boron, Veeman et al. made the observation that framework boron appears to be able to switch from tetrahedral to trigonal coordination on dehydration.[38] Boron coordinated to silicon in glasses, minerals, or zeolites is shielded by up to ~4 ppm from tetrahedral borates,[39] and can often be identified on this basis. The chemical shifts and quadrupole coupling constants of many borates and borosili-

For References see p.2658

cates have now been determined, and typical values are given in Table 3.

Another class of boron containing materials of considerable technological interest are the boroaluminate glasses. These have been investigated by using ^{11}B and ^{27}Al NMR spectroscopy, and evidence for both three- and four-coordinate boron, as well as four-, five- and six-coordinate aluminum, has been obtained, and data analyses based on the presence of all species present, combined with local charge balance considerations, correctly predict compositional variations of both ^{11}B and ^{27}Al NMR parameters over a wide glass compositional range.[40]

As well as B in oxidic environments, ^{11}B (and ^{13}C) MAS NMR has been used to probe the highly complex B–C phase diagram.[41] When combined the NMR results indicate that:

a) the B_4C composition appears to be the most ordered and contains essentially only $B_{11}C$ icosahedra (see *Icosahedron*) and C–B–C intericosahedral chains;
b) the extent of B/C order decreases with increasing B content;
c) the $B_{13}C_2$ composition is not fully ordered and has about 10% of its C in icosahedra;
d) the excess B over the B_4C composition appears to substitute preferentially for C in the icosahedral positions relative to the chain positions.[41]

2.7 Spin-Echo NMR

The NMR spectra of most quadrupolar nuclei are broadened by the interaction of the nuclear quadrupole moment (eQ) with the electric field gradient at the nucleus (eq), giving rise to splittings of the Zeeman lines or, in random powders, to broad powder pattern lineshapes. In pulsed NMR, broad lines cause difficulties associated with finite spectrometer recovery times, which can lead to gross spectral distortions. One potential route around this problem is to use a second, refocusing pulse, and generate a so-called spin-echo. If data acquisition is begun at the top of an echo, then lineshape distortions are minimal. A potential problem in spin-echo studies of some quadrupolar nuclei in solids is that a series of echoes may be obtained. Solomon first reported[42] the refocusing of first-order quadrupolar interactions, in $K^{127}I$. Although in some cases multiple echoes can be detected, by using a phase shifted pulse sequence the 2τ echo is usually the only one observed, and a Fourier transform of the echo can yield an essentially undistorted first-order powder spectrum.[43] Figure 4a shows a ^{27}Al spin-echo for a 1:1 mole ratio mixture of $KAl(SO_4)_2 \cdot 12H_2O$ and $NH_4Al(SO_4)_2 \cdot 12H_2O$, in the presence of ^1H dipolar decoupling, and Figure 4b the Fourier transform of the half-echo. There are clearly two overlapping $I = \frac{5}{2}$ powder patterns, characterized by slightly different e^2qQ/h values. Using a numerical method it is possible to deconvolute the random powder lineshape, resulting in well resolved $\pm\frac{1}{2} \leftrightarrow \pm\frac{3}{2}$ and $\pm\frac{3}{2} \leftrightarrow \pm\frac{5}{2}$ satellite transitions, corresponding to $e^2qQ/h \approx 395$ kHz (K^+ alum) and $e^2qQ/h \approx 441$ kHz (NH_4^+ alum). Equivalent results have been obtained by using a so-called zero-field (field cycling) approach.[44]

This spin-echo approach is limited to systems in which relatively uniform excitation of all spin transitions can be achieved, which for many quadrupolar nuclei is impractical. However, for large e^2qQ/h values (which is often the case found experimentally, e.g. in ^{17}O NMR of the silica/silicate/zeolite systems) the essentially opposite approach, that of using very weak or soft pulse excitation of solely the $\frac{1}{2}, -\frac{1}{2}$ transition, can be very effective. Figure 5a shows a one-pulse experiment on ^{39}K in an 18-crown-6 ether·KNO_3 complex (see *Crown Ethers*), at 11.7 T (corresponding to a ^{39}K resonance frequency of 23.33 MHz).[45] Such low Larmor frequencies generally cause problems with pulse feedthrough due to long ringdown time constants,

Table 3 Boron-11 Nuclear Quadrupole Coupling Constant and Chemical Shift Data for Borates and Borosilicates[a]

Sample	Formula	Boron-11 NMR parameters			
		Trigonal		Tetrahedral	
		QCC (MHz)	δ_{iso} (ppm)[b]	QCC (MHz)	δ_{iso} (ppm)[b]
Boracite	$Mg_3B_7O_{13}Cl$	2.6	16.0	~0.3	1.0
Colemanite	$CaB_3O_4(OH)_3 \cdot H_2O$	2.4	17.0	~0.3	1.4
Danburite	$CaB_2Si_2O_8$	–	–	~0	~0.7
Datolite	$CaB(SiO_4)(OH)$	–	–	~0	1.0
Inderite	$MgB_3O_3(OH)_5 \cdot (H_2O)_4 \cdot H_2O$	2.4	18.1	~0.2	1.0
Inyoite	$CaB_3O_3(OH)_5 \cdot 4H_2O$	2.3	17.4	~0.2	1.5
Kernite	$Na_2B_4O_6(OH)_2 \cdot 3H_2O$	2.4	18.5	~0.2	0.9
Tourmaline	$(Na, Ca)(Li, Mg, Al)(Al, Fe, Mn)_6(BO_3)_3(Si_6O_{18})(OH)_4$	–	12.7	–	–
Ulexite	$NaCaB_5O_6(OH)_6 \cdot 5H_2O$	2.45	18.2	~0.3	1.2
Boron phosphate	BPO_4	–	–	0	−3.3
Lithium borate	$Li_2B_4O_7$	2.5	17.9	~0.2	1.7
Potassium pentaborate	$K_2B_{10}O_{16} \cdot 8H_2O$	2.5	18.9	~0.3	1.4
Borax	$Na_2B_4O_7 \cdot 10H_2O$	2.4	19.0	~0.3	2.0
Pyrex (1)		2.5	12.6	~0.5	1.8
(2)		2.3	16.0	~0.5	0.2
Reedmergnerite	$NaBSi_3O_8$	–	–	~0	−1.9
Alkali feldspar	$NaAl(B)Si_3O_8$	–	–	~0	−1.1
					−2.5

[a]Adapted from Turner et al.[39] [b]From $BF_3 \cdot Et_2O$.

List of General Abbreviations on back endpaper

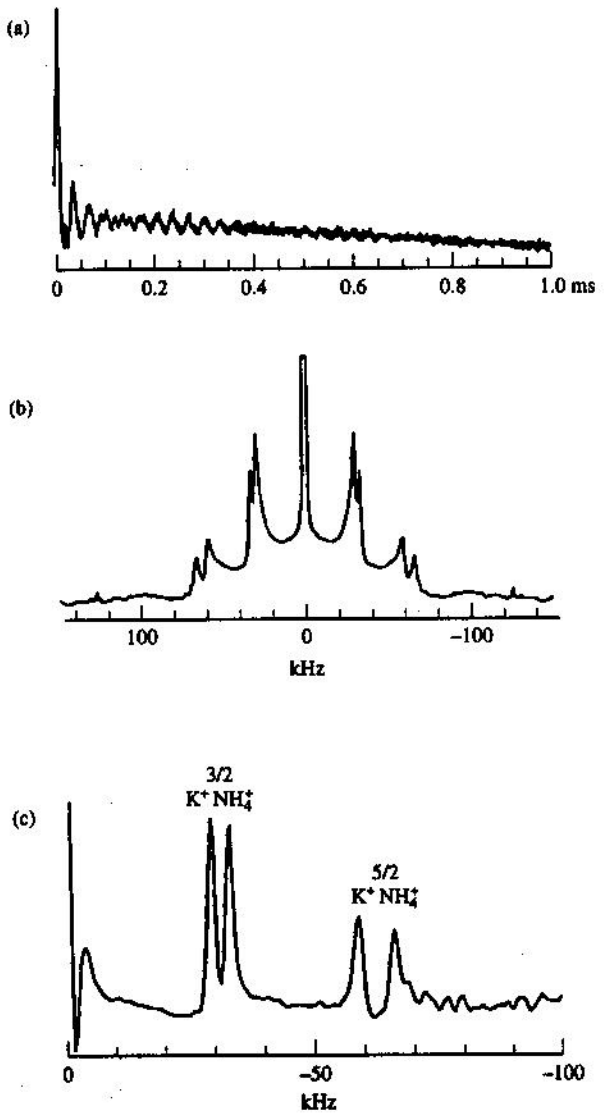

Figure 4 Aluminum-27 quadrupole-echo NMR spectra of a 1:1 molar mixture of $KAl(SO_4)_2{\cdot}12H_2O$ and $NH_4Al(SO_4)_2{\cdot}12H_2O$, obtained at a magnetic field strength of 3.52 T, in the presence of ^1H dipolar decoupling: (a) ^{27}Al spin-echo; (b) Fourier transform of half-echo showing central $(\frac{1}{2}, -\frac{1}{2})$ and overlapping satellite $(\frac{1}{2}, \frac{3}{2}; \frac{3}{2}, \frac{5}{2})$ transitions for the K^+ and NH_4^+ alums; (c) deconvoluted version of (b) showing complete resolution of both K^+ and NH_4^+ alums in both satellite transitions, corresponding to $e^2qQ/h \approx 395$, 441 kHz, η assumed ≈ 0. (Reproduced by permission of Macmillan from Oldfield et al.[43])

and as can be seen in Figure 5a the ^{39}K spectrum is hardly visible over the pulse breakthrough artifact. However, use of a 'Hahn' spin-echo (equation 6):

$$(\theta_1)\phi_1 - \tau_1 - (\theta_2)\phi_2 - \tau_2 - (\mathrm{AQ})\phi_3 \qquad (6)$$

combined with the phase cycle shown in equation 7:

$$\begin{aligned}\phi_1 &= xxxx\ yyyy\ \overline{xxxx}\ \overline{yyyy}\\ \phi_2 &= xy\overline{xy}\ xy\overline{xy}\ xy\overline{xy}\ xy\overline{xy}\\ \phi_3 &= \overline{yyyy}\ \overline{xxxx}\ yyyy\ xxxx\end{aligned} \qquad (7)$$

has the effect of canceling any free induction decay contribution to the echo (Figure 5b), which after Fourier transformation yields a well resolved second-order powder pattern lineshape (Figure 5c), from which $e^2qQ/h = 1.80$ MHz, $\eta = 0.37$, and $\delta_{iso} = 0$ ppm can be derived (Figure 5d). Thus, the Hahn spin-echo method permits the recording of undistorted powder pattern lineshapes, much as the solid echo technique has been used to record ^1H or ^2H NMR spectra.

After excitation, the spin-echo decays with a time constant T_{2H}, and measurement of T_{2H} values leads to a new spectroscopic parameter with which to investigate quadrupolar nuclei in inorganic solids.[46] The response to spin-echo radiofrequency (rf) pulse excitation of a variety of nonintegral spin quadrupolar nuclei (^{23}Na, ^{27}Al, and ^{93}Nb) in inorganic solids (single crystal ruby and sapphire, α-Al_2O_3, γ-Al_2O_3, AlN, $NaNO_3$, $KNbO_3$, $NaNbO_3$, $LiNbO_3$, albite, and the zeolite Linde A) subject to strong quadrupolar interactions and dipolar interactions of varying strength, has been reported.[46] It has been demonstrated that 'soft' rf pulse excitation with a pair of selective $\pi/2$ and π pulses yields predictable spin-echo decay behavior as a function of dipolar interaction. The experimental results are in good agreement with the theoretical predictions. In particular, the $1/e$ decay time constant for a Gaussian decay of the spin-echo, T_{2E}, has been shown (equation 8) to be:

$$T_{2E} = \sqrt{2/(M_{2E}(I) + M_{2E}(S))} \qquad (8)$$

where $M_{2E}(I,S)$ are the second moments of the spin-echo decay for a heteronuclear dipolar coupled spin system. If heteronuclear dipolar coupling is negligible, then the decay can be approximated by equation 9:

$$T_{2E} = \sqrt{2/M_{2E}} \qquad (9)$$

Experimentally, it is found that T_{2H} values vary widely depending on the strength of the dipolar interactions present. This can be used to advantage in determining local environments in complex systems. For example, in zeolites (see ***Zeolites***) used in the petrochemicals industry as cracking catalysts, zeolitic Al levels are relatively low (typically ≤0.1 wt %), while aluminum levels in binder materials (such as γ-Al_2O_3, or clay-based materials) are much higher, of the order of 20–40 wt %. It is thus difficult to observe the catalytically relevant zeolitic sites in a typically formulated catalyst, since their tetrahedral Al are 'buried' under a 10^2 or 10^3 fold larger binder signal. However, in the magnetically dilute zeolites, T_2 values are much longer than those associated with the aluminaceous binders, so that the binder signal can be completely 'edited' away by using a two-pulse in-phase Hahn spin-echo.

For References see p.2658

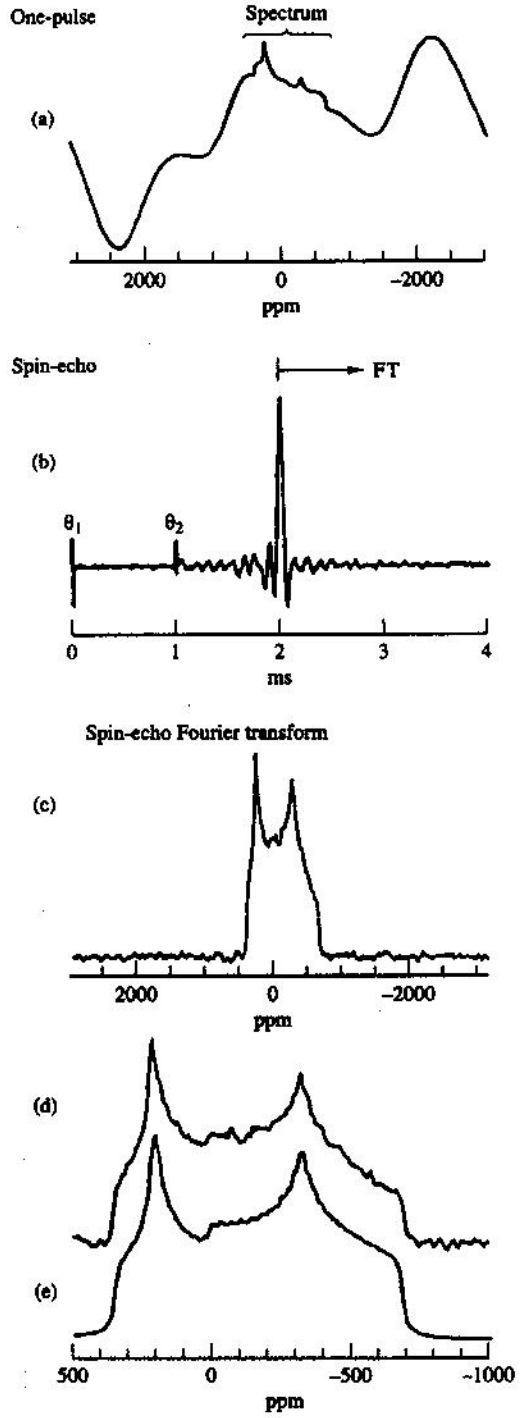

Figure 5 Potassium-39 NMR spectra of 18-crown-6 ether·KNO_3 complex at 11.7 T: (a) one-pulse experiment (pulse width of 7.4 μs, corresponding to a 90° pulse for the solid); (b), time domain response using a first pulse width = 3.7 μs, second pulse = 7.4 μs, τ_1 = 1 ms. In this experiment, for demonstrating the suppression of the FID due to use of two pulses, data acquisition was begun immediately after the first pulse. The echo-maximum occurs at about 2 ms. (c) Fourier transform of the (half) echo in (b). The unusually large τ_1 value required to suppress all ringing results in a spectrum with a somewhat poorer signal-to-noise ratio than is normally achievable. (d) Expansion of spectrum in (c). (e) Simulation of spectrum in (d) using e^2qQ/h = 1.80 MHz, η = 0.37, and δ_{iso} = 0 ppm. (Reproduced by permission of Academic Press from Kunwar et al.[45])

List of General Abbreviations on back endpaper

2.8 Signal Quantitation

For nonintegral spin quadrupolar nuclei, considerable care needs to be taken when 'counting spins', since the exact nature of the excitation used has a major influence on the results obtained. The results of calculations of the intensities of the central and satellite transitions for quadrupolar nuclei under various types of rf excitation have been given by Fukushima and Roeder.[47] Freude et al.[48] confirmed these theoretical predictions using an aqueous aluminum salt solution as an external spin-counting standard, and showed that as expected a maximum intensity of the $\frac{1}{2}$, $-\frac{1}{2}$ spin transition in Al_2O_3 was obtained by using a 90° pulse having a width $1/\sqrt{(I(I+1) - m(m+1))}$ or $\frac{1}{3}$ that of a solution standard.[48] These results can be applied to other quadrupolar nuclei as well, e.g. a ^{11}B ($I = \frac{3}{2}$) solids-90 is half the solution 90° pulse length; a ^{133}Cs ($I = \frac{7}{2}$) solids-90 is one-quarter the solution 90° pulse length, etc. For two-pulse spin-echo NMR, signal quantitation is more complex, since the second pulse can give rise to mixing of the different spin states, and it has been found to be generally most accurate to use extremely weak or selective pulse excitation, so that only the central ($\frac{1}{2} \leftrightarrow -\frac{1}{2}$) spin transition is excited, and observed. Selective excitation is achieved by lowering the transmitter rf power such that solid 90° pulse widths of ~40 μs are used, in which case excellent quantitation can usually be achieved.

2.9 Spin–Lattice Relaxation

In liquid state NMR, the spin–lattice relaxation times of quadrupolar nuclei are almost always short, due to very efficient quadrupolar relaxation. This is brought about by random thermal motions, and the fluctuating electric field gradients at the nucleus cause rapid spin–lattice relaxation. In inorganic solids, however, there is usually little motion, and so there are few relaxation pathways. While phonon assisted modes may be important at very low temperatures, they play only a small role at room temperature, where T_1 relaxation times of many seconds, or even minutes, are often observed. Thus spin–lattice relaxation can be dominated by paramagnetic impurity centers (e.g. Fe^{3+}), and use of T_1 as a structural probe has therefore been quite limited.

There are two main exceptions to the above, in which either molecular/ion motion, or conduction electron spins, play an important role in T_1 relaxation. In some inorganic solids, water or ion motions provide an efficient pathway to spin–lattice relaxation by causing a fluctuating electric field gradient at the nucleus. In zeolites, for example, there is no correlation between T_1 and the static part of the electric field gradient (which gives rise to the observed e^2qQ/h value); however, the fluctuating part, $eq(t)$ due to ion and water (dipole) motion gives rise to rapid spin–lattice relaxation. In ^{17}O-labeled zeolites and Ga-analog zeolites, it was shown that all experimental T_1 data (on ^{17}O, ^{23}Na, ^{27}Al, and ^{71}Ga) could be fitted by a single model in which $eq(t)$ for each nucleus was assumed to be the same, i.e. a single physical process was responsible for relaxation of all framework and nonframework species.[49] Spin–lattice relaxation in glassy ***Ionic Conductors*** has also been investigated, and ion

motion has been shown to be an important relaxation mechanism in these materials as well.[50]

A second class of conductors in which spin–lattice relaxation is very efficient are the so-called high transition temperature (high T_c) oxide superconductors (see *High Temperature Superconductivity*). In these materials, typified by the phase $YBa_2Cu_3O_{7-x}$, the relaxation rates (and Knight shifts) of ^{17}O, $^{63,65}Cu$, as well as $^{135,137}Ba$, have all been investigated, as has the $I = \frac{1}{2}$ ^{89}Y relaxation. Of particular interest has been the observation of near Korringa relaxation for oxygen sites, where the Korringa relation (equation 10)

$$K^2 T_1 T \left(\frac{\gamma_n}{\gamma_e}\right)^2 \frac{4\pi k_B}{\hbar} = 1 \qquad (10)$$

relates T_1 and the Knight shift, K, while Cu relaxation is dominated by antiferromagnetic spin fluctuations (see *Antiferromagnetism*).[51] The Cu, O, Y relaxation rates have been explained in terms of so-called form factors, which describe how Cu spin fluctuations affect the nucleus under observation. For example, the close-to-Korringa relaxation at oxygen can be thought of as being due to a cancellation of Cu spin fluctuations due to antiferromagnetic coupling across oxygen (Cu↑–O–Cu↓). The interested reader is referred to the extensive solid state physics literature on these topics for further details (e.g. Pennington and Slichter[51]).

2.10 Cross Polarization to Quadrupolar Nuclei

The Hartman–Hahn–Lurie–Slichter cross-polarization technique developed by Pines, Gibby, and Waugh[52] has found extensive use in the area of solid state ^{13}C NMR, and while cross-polarization experiments involving polarization transfer from ^1H to spin-$\frac{1}{2}$ nuclei such as ^{15}N, ^{29}Si, ^{31}P, and ^{113}Cd have also now become routine, there have been few reports of cross polarization from ^1H to quadrupolar nuclei, where the cross-polarization process is more complicated than with $I = \frac{1}{2}$ systems. For example, for integer spin nuclei such as ^{14}N ($I = 1$), the cross-polarization match condition differs for different orientations in a polycrystalline sample, and can lead to distorted spectra. In general, the match condition is given by equation 11:

$$\alpha_a \gamma_a H_{1a} = \alpha_b \gamma_b H_{1b} \qquad (11)$$

where γ_i and H_{1i} are the gyromagnetic ratio and rf field strength for nucleus i, and $\alpha = [I(I+1) - m(m-1)]^{1/2}$ for a transition between levels m and $(m-1)$. When both nuclei have $I = \frac{1}{2}$, this equation reduces to the familiar form $\gamma_a H_{1a} = \gamma_b H_{1b}$. However, for ^1H cross polarization of the $(\frac{1}{2}, -\frac{1}{2})$ transition of e.g. ^{17}O ($I = \frac{5}{2}$), the match condition will be $3\gamma_O H_{1O} = \gamma_H H_{1H}$, from equation 11. These conditions amount to matching the ^1H 90° pulse length to the 'solid' ^{17}O 90° pulse length, which is smaller than the solution value by the same factor α. For example, with a ^1H 90° pulse length of 5 μs ($\gamma_H H_{1H}$ = 50 kHz) one observes optimum cross polarization when $\gamma_O H_{1O}$ = 16.7 kHz, which corresponds to a 'solution' ^{17}O 90° pulse length of 15 μs, but to a 'solid' ^{17}O 90° pulse length of 5 μs.[26]

Cross-polarization ^{17}O NMR spectra of a variety of ^{17}O-labeled solids ($Mg(OH)_2$, $Ca(OH)_2$, boehmite (AlO(OH)), talc, Ph_3SiOH, and amorphous SiO_2) have been reported using high-field static and MAS techniques, which show that large cross-polarization enhancements can be obtained, and second-order quadrupolar powder lineshapes observed, under cross-polarization conditions. For example, in talc ($Mg_3Si_4O_{10}(OH)_2$), cross polarization permits editing of the MgOH oxygen resonances (which cross polarize) from the SiOMg and SiOSi oxygen sites (which do not cross polarize appreciably using short mix times), thereby simplifying the analysis of the ^{17}O NMR spectrum of this sheet silicate.[26] ^{17}O MAS and CP-MAS NMR spectra of ^{17}O-labeled boehmite (AlO(OH)), bayerite ($Al(OH)_3$), and several transitional aluminas have also been reported.[53] Cross polarization from ^1H to ^{17}O has been used to enhance the hydroxyl oxygen resonances of boehmite and bayerite, and to allow the observation of hydroxyl groups on the surface of γ-Al_2O_3. The spectra yield nuclear quadrupole coupling constants, electric field gradient tensor asymmetry parameters, and isotropic chemical shifts for each chemically distinct oxygen site. The quadrupole coupling constants for tetrahedrally coordinated oxide sites (OAl_4) range from 1.2 to 2.2 MHz, while those of trigonally coordinated hydroxide sites (Al_2OH) are in the 5–6 MHz range. Trigonally coordinated oxide sites (OAl_3), arising as a result of cation vacancies (see *Vacant Site*) in the transitional aluminas, have quadrupole coupling constants of approximately 4 MHz, and it has been shown that the observed quadrupole coupling constants and asymmetry parameters are in good agreement with the results of electric field gradient calculations based on point charge models.[53]

Cross polarization has been observed not only from ^1H to ^{17}O, but also with a number of other quadrupolar nuclei. For example, both $^{31}P \rightarrow {}^{27}Al$ and $^{27}Al \rightarrow {}^{31}P$ CP of $AlPO_4$-n materials are possible, and use of rapidly relaxing ^{27}Al nuclei to cross polarize more slowly relaxing $I = \frac{1}{2}$ ^{31}P nuclei enables rapid data acquisition. This basic idea has been extended to cross polarization between pairs of quadrupolar nuclei, e.g. $^{27}Al \rightarrow {}^{17}O$ in α-Al_2O_3, and in Linde A and Linde Y zeolites. When two quadrupolar nuclei are involved, lineshape distortions become significant when two second-order powder patterns need to be Hartman–Hahn matched.

Other double resonance techniques, based on coherence transfer via weak heteronuclear dipolar interactions, e.g. between ^{27}Al and ^{31}P, also show great promise for determining through-space correlations,[54] which can then be used to establish three-dimensional connectivities in complex materials.

2.11 Satellite Transition and Nutation NMR

The MAS NMR studies discussed above were concerned primarily with the observation of $\frac{1}{2}$, $-\frac{1}{2}$ transitions of nonintegral spin quadrupolar nuclei. However, recent developments in the design of very fast (~15–20 kHz) and stable (±5 Hz) MAS probes, combined with fast recovery electronics, has now

For References see p.2658

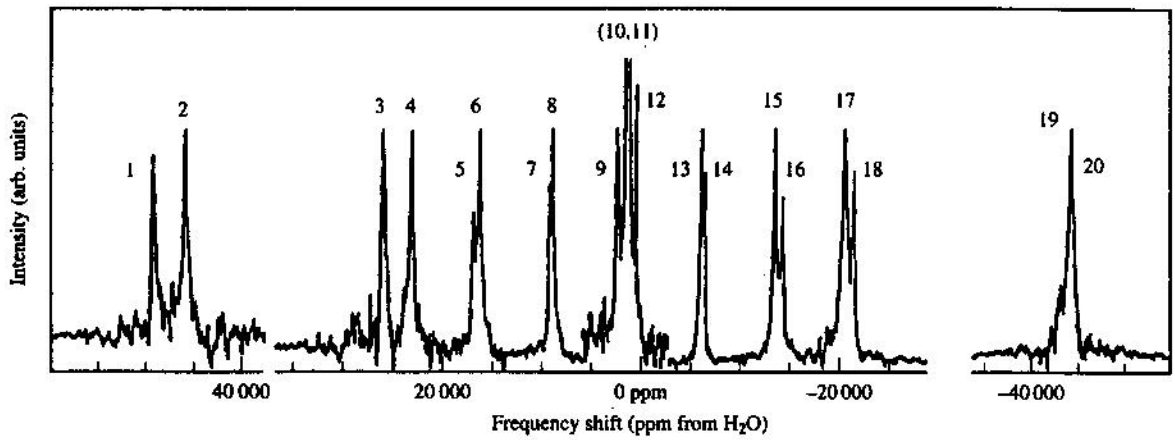

Figure 6 Oxygen-17 NMR spectra of magnetically aligned $YBa_2Cu_3O_{7-x}$ ($H_0 \| c$), at 8.45 T and 300 K. The peak intensities have been equalized for clarity. The actual intensities for central and satellite transitions have the appropriate 9:8:5 relative intensity ratios. 19 of the possible 20 transitions (four oxygens × five transitions) can be observed; the central transitions for O(2,3) overlap. Connectivities for the individual sites are as follows: O(1), peaks 2, 4, 12, 18, 19; O(2,3), peaks 5–8, (10,11), 13–16; O(4), peaks 1, 3, 9, 17, 20. (Reproduced by permission of the American Institute of Physics from Oldfield et al.[28])

allowed determination of complete (central and satellite transition) MAS NMR spectra, e.g. of α-$^{27}Al_2O_3$ and $^{23}NaNO_3$,[55] or determination of both quadrupole and anisotropic chemical shielding tensors, including the relative orientation of their principal axis systems, e.g. in $NH_4{}^{51}VO_3$ and $^{51}V_2O_5$.[56]

A second method which has been frequently used to determine e^2qQ/h and η values is the nutation method of Lippmaa et al.,[8] which allows an alternative separation of the chemical shift and quadrupole interaction. The method is based on the evolution of the spin system in a weak rotating B_1 field, but has the sensitivity of high-field NMR, and yields a so-called nutation spectrum.[57] A series of reference nutation spectra for $I = \frac{3}{2}, \frac{5}{2}, \frac{7}{2}$, and $\frac{9}{2}$ has been published,[57] and applied to ^{27}Al in spodumene, and ^{45}Sc in $Sc_2(SO_4)_3$.

2.12 Single Crystal NMR

In early work, many groups used continuous wave wide-line NMR methods to investigate quadrupolar nuclei in single crystals. Of particular interest were minerals, of which large well formed crystals can often be obtained. Single crystal studies, where feasible, are highly informative, since complete electric field gradient tensors can be determined.[58] When single crystals are too small to give adequate signal-to-noise ratios, large arrays of individually aligned microcrystals have been used, e.g. to observe $^{63,65}Cu$ and ^{17}O NMR in $YBa_2Cu_3O_{7-x}$.[59] When crystals are too small for mechanical alignment, the magnetic alignment method described in Section 2.13 may be of use.

2.13 Magnetic Alignment

Particles having a large anisotropy in their diamagnetic or paramagnetic susceptibility experience a large torque when placed in a magnetic field, and this force tends to orient or align them in that field. The (nuisance) effects of partial magnetic alignment have been known in *Electron Paramagnetic Resonance* of powders for many years, but more recently have been put to good use in solid state NMR, e.g. to align proteins, DNA, lipid membranes, and high temperature superconductors.[28] In the oxide superconductors, microcrystals are suspended in epoxy resin, then placed into a strong magnetic field. The crystals align (with B_0 parallel to the crystallographic c axis in $YBa_2Cu_3O_{7-x}$), and although randomly oriented about c, samples give rise to a (pseudo) single crystal NMR spectrum. A typical result is shown in Figure 6 in which almost all 20 lines expected can be observed (the $\frac{5}{2}, \frac{3}{2}, \frac{3}{2}, \frac{1}{2}, \frac{1}{2}, -\frac{1}{2}, -\frac{1}{2}, -\frac{3}{2}$, and the $-\frac{3}{2}, -\frac{5}{2}$ transitions of the two planar, the chain, and the apical oxygen). Each line experiences a measurable second-order quadrupolar shift, and from measurements at two or more magnetic field strengths the electric field gradient and Knight shift tensor elements at each site can be determined. Similar magnetically ordered spectra of $^{63,65}Cu$, $^{135,137}Ba$, and ^{89}Y have all been reported for $YBa_2Cu_3O_{7-x}$, and its oxygen-deficient relatives, and electric field gradient and Knight shift parameters determined.[28,51,58]

2.14 Other Quadrupolar Nuclei

There are many other NMR-accessible quadrupolar nuclei in the Periodic Table which have nonzero spin but which have not been discussed above, since they have a much less frequent occurrence in inorganic chemical systems. Examples include ^7Li, ^9Be, ^{25}Mg, ^{33}S, $^{35,37}Cl$, ^{45}Sc, $^{47,49}Ti$, ^{67}Zn, ^{73}Ge, ^{79}Br, ^{87}Sr, ^{91}Zr, ^{115}In, and ^{139}La. There are also large numbers of other possible quadrupolar candidates, but they are usually either radioactive, or have very large quadrupole moments or very low sensitivities, or are of limited interest to most chemists.

List of General Abbreviations on back endpaper

3 SPIN $I = \frac{1}{2}$ SYSTEMS

Spin $I = \frac{1}{2}$ nuclei have no nuclear quadrupole moment, and although rare in the Periodic Table, the frequent occurrence of ^{1}H, ^{13}C, ^{15}N, ^{19}F and ^{29}Si in inorganic solids, together with the relatively high sensitivity and resolution obtainable with most of these nuclei, means that a large body of information exists on them.[12,13] The most sensitive nuclei are ^{1}H and ^{19}F. While usually a blessing, nuclei with large gyromagnetic ratios when present in the solid state in high concentrations experience large homonuclear dipolar interactions, which give rise to extreme spectral broadening. For example, a CH_2 group or H_2O molecule has an ~80 kHz ^{1}H–^{1}H dipolar interaction, which only averages under MAS under the condition that it is an 'inhomogeneous' interaction, e.g. as found with isolated spin pairs. For most real systems having multiple H–H or F–F interactions (e.g. ice, CaF_2), spinning at very high speeds, or application of a multiple pulse train (to average the dipolar interaction) combined with MAS, is required in order to get even moderate resolution.[13,60] There have thus been few applications, and most interest has focused on the magnetically dilute systems ^{13}C, ^{29}Si, and ^{31}P, with additional but rarer applications to heavy metals (e.g. ^{113}Cd and ^{183}W) also having been reported. We thus begin our description of the $I = \frac{1}{2}$ systems with the most studied nuclei, then follow this with a brief discussion of some of the more difficult nuclei.

3.1 Silicon-29 NMR

Silicon-29 has a natural abundance of 4.7% and resonates at 99.3 MHz at 11.7 T (a 500 MHz ^{1}H resonance frequency), and is thus moderately sensitive. The lack of direct Si–H bonds in most inorganic materials, and the small CSA due to approximately tetrahedral symmetry, means that silicon NMR spectra can be obtained without ^{1}H decoupling or cross polarization, even at slow (~2–3 kHz) MAS rates, so only simple NMR instrumentation was required in order to obtain the first high-resolution ^{29}Si MAS NMR spectra of inorganic solids,[5] and several good accounts are available which deal extensively with this topic.[12,13]

One of the most useful aspects of ^{29}Si NMR is that the ^{29}Si chemical shift is very sensitive to the bonding around a given SiO_4 tetrahedron. In simple silicates there are five types of bonding: mono- or nesosilicates (Q^0) having no Si–O–Si bonds, such as forsterite (Mg_2SiO_4); di- or sorosilicates (Q^1), having one Si–O–Si bond; chain or inosilicates (Q^2) having two Si–O–Si bonds, such as diopside ($CaMgSi_2O_6$); sheet or phyllosilicates (Q^3) having three Si–O–Si bonds, such as talc ($Mg_3Si_4O_{10}(OH)_2$); and framework or tectosilicates (Q^4) having four Si–O–Si bonds, such as quartz (SiO_2). A second class of Q^2-containing silicates are the cyclosilicates, such as $K_4H_4Si_4O_{12}$. For the most part the chemical shift ranges occupied by each of the five silicate classes do not overlap (Figure 7a),[61] which permits a good estimate of the type of silicate environment present in a material of unknown structure. Upon substitution of Al for Si in the sheet or framework materials, such as clays and zeolites, there is a decrease in shielding for each Al (and counterion) added. Figure 7b shows the entire series of Q^4 chemical shift ranges:[13] $Q^4(0Al)$, $Q^4(1Al)$, $Q^4(2Al)$, $Q^4(3Al)$, and $Q^4(4Al)$. While there are clearly overlaps in a given material, such as a Linde X or Y zeolite, there is usually good separation between the $Q^4(n\text{Al})$ sites, and results for Linde A and Y are shown in Figure 8. If the $Q^4(n\text{Al})$ sites can be assigned, and in the absence of Al–O–Al groups (Loewenstein's rule[12,13]), then the Si:Al ratio in framework or layer silicates can be deduced from measurements of the intensities of the $Q^4(n\text{Al})$ resonances.[12,13] This type of measurement is now routinely used in the characterization of zeolite materials. Moreover, in addition to permitting an analysis of Si:Al ratios, ^{29}Si NMR often permits a determination of Si,Al ordering, e.g. in layer silicates, feldspars, and zeolites.[13] The reason for this is that a given random or nonrandom arrangement of Al atoms will give rise to a predictable pattern of $^{29}SiO_4(n\text{Al})$ peak intensities. However, ^{29}Si NMR can only rigorously disprove a random pattern of ordering; it cannot prove an ordering model in the absence of additional information.[13]

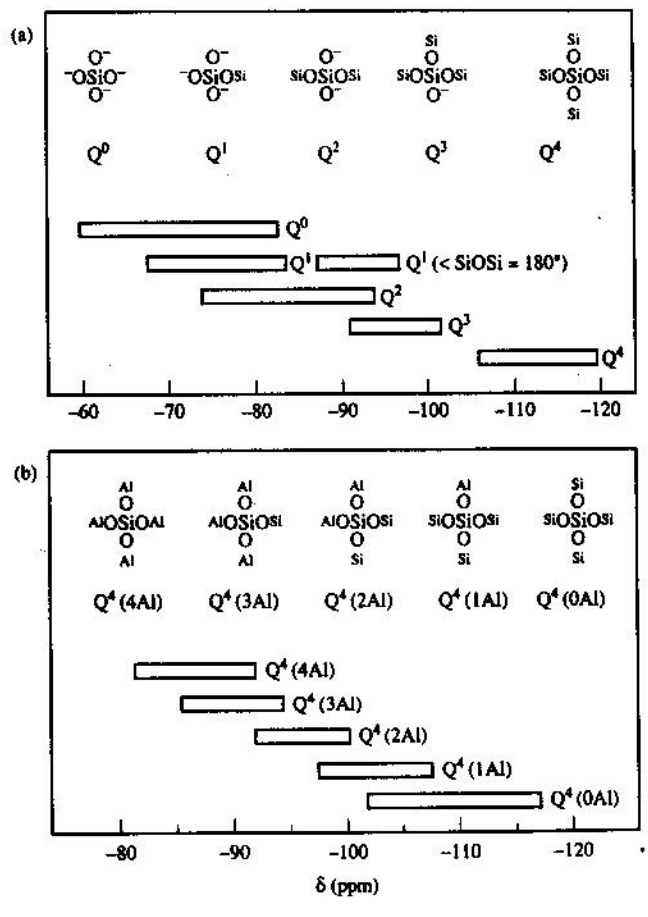

Figure 7 Silicon-29 isotropic chemical shift ranges in silicates (Q^0–Q^4) and framework aluminosilicates ($Q^4(4Al)$–$Q^4(0Al)$). (Adapted from Engelhardt and Michel[13])

In addition to the large effects due to SiOSi or SiOAl bonding, ^{29}Si NMR is an important probe of crystallographic

For References see p.2658

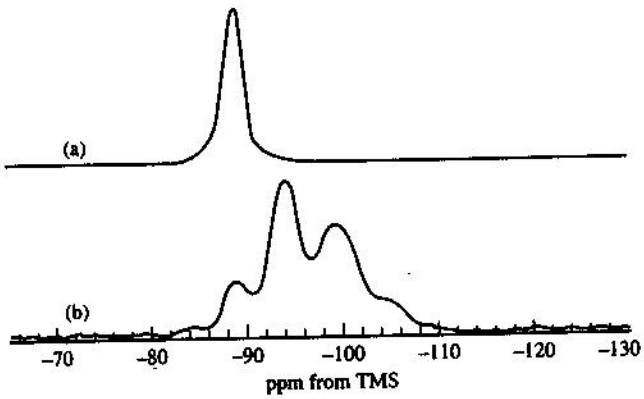

Figure 8 Silicon-29 MAS NMR spectrum of Linde A, Linde Y zeolites, at 8.45 T: (a) Linde A; (b) Linde Y

site nonequivalence. This is dramatically shown in the case of the zeolite ZSM-5,[62] which under certain synthesis conditions approaches the empirical formula SiO_2. However, there may be 12 or 24 crystallographically and magnetically nonequivalent sites in ZSM-5, and Fyfe et al. showed that a low Al content ZSM-5 gives up to 24 ^{29}Si resonances[12,13] covering an ~7 ppm chemical shift range (Figure 9a). Assignment of these peaks represented a major challenge, but was successfully accomplished by using ^{29}Si-enriched materials and a 2D NMR (INADEQUATE) technique[62]; a typical 2D result is shown in Figure 9b. Since this material is substantially aluminum free, the chemical shift nonequivalencies exhibited are a result of changes in the electronic wavefunctions (see *Wavefunction*) at Si due to crystallographically imposed bond angle and *Bond Length* restraints. This type of nonequivalence has been observed in numerous framework silicates, and ~20 empirical correlations between T–O–T bond angle and chemical shift, as well as Si–O bond length and chemical shift, have been proposed.[12,13]

The actual origins of the chemical shifts observed in silicates requires in principle the application of ab initio quantum chemical techniques, which themselves require a detailed knowledge of the bond lengths and bond angles involved, as well as solution of the problem of the electrostatic charge field around silicon, and an ability to handle very large basis sets for Si, Ca, Ba, etc. Fortunately, much simpler empirical approaches to estimating chemical shifts in silicates already exist, although the ab initio methods can be expected to improve on the empirical methods in the future. One such empirical method is the group *Electronegativity* sum approach.[63] Linear relations between group electronegativity (EN) sums of ligands bonded to tetravalent silicon and silicon-29 chemical shifts have been shown (equation 12) to exist:

$$\delta(\mathrm{Si, ppm}) = -24.336 \sum \mathrm{EN} + 279.27 \qquad (12)$$

This correlation has been applied to many silicates and aluminosilicates (containing insular (Q^0) to framework (Q^4) Si sites) to predict silicon-29 NMR chemical shifts, where all fragments (e.g. OAl, OLi, OCa) attached to Si are assigned (on the basis of experiments on a series of model silicates and equation 12) a characteristic group (or fragment) electronegativity value. OSi group electronegativities were scaled linearly with bridging bond angle. As an example of the use of the method, the electronegativity sum value for the cyclosilicate (Q^2) beryl ($Al_2Be_3(SiO_3)_6$) can be derived as EN(OBe) + EN(OAl) + 2(EN(OSi) (168.2°)) = 15.67, which predicts a silicon-29 chemical shift of −102.1 ppm (from Me_4Si). This compares favorably with the experimental result, $\delta_{iso} = -102.6$ ppm. On the basis of a total of 99 sites in 51 different compounds, the mean absolute deviation between theory and experiment is <2 ppm,[63] and the group electronegativity sum method appears to be one of the most accurate methods of predicting silicon-29 chemical shifts found to date, when all types of silicate are considered.

In addition to the many studies of SiO_4 tetrahedra in silicates, ^{29}Si MAS NMR has also been found to be a valuable spectroscopic probe of the more unusual six-coordinate silicates found in synthetic high-pressure phases[64] or in phosphosilicates.[65] The main Si^{VI} containing phase is stishovite, which has a chemical shift $\delta_{iso} = -191$ ppm from TMS, a value which becomes even more shielded in the phosphosilicates, $\delta_{iso} \approx -212$ ppm.[65] ^{29}Si NMR has also been investigated in many inorganic solids by using the ^1H cross-polarization method described in Section 2.10 quadrupolar nuclei; of particular interest has been the characterization of surface silanol (SiOH, $Si(OH)_2$) species in high surface area silicas.[13]

3.2 Carbon-13 NMR

While most ^{13}C NMR studies clearly fall outside the area of inorganic chemistry, ^{13}C MAS NMR has been found to be of use in the area of metal carbonyl and surface organometallic chemistry. Four main areas have been investigated: metal complexes grafted on to oxide supports, organometallic complexes trapped in zeolite cages, supported metal alkenes, and small molecules (CO, C_2H_4) directly bonded on to supported metal catalysts.

A number of workers have investigated the ^{13}C static and MAS NMR of solid transition metal carbonyls. A large amount of shielding tensor data has been accumulated,[66] and interesting information, e.g. on fluxionality (see *Fluxional Molecule*) in the solid state, has been obtained.[67,68] Both the isotropic chemical shift, as well as the shift anisotropy, help differentiate terminal from bridging (μ_2, μ_3) CO ligands (see *Bridging Ligand*), and in some cases the effects of J and dipolar coupling can be detected, facilitating spectral assignments.[69]

In surface organometallic chemistry, the reaction between $Mo(CO)_6$ and γ-Al_2O_3 has been extensively studied, and evidence obtained for mobile (physisorbed) $Mo(CO)_6$, a rotating $Mo(CO)_5$–surface species, and a more rigid $Mo(CO)_3$–surface species. The interactions of $Os_3(CO)_{12}$, $H_2Os(CO)_4$, $H_4Os_4(CO)_{12}$, $Rh(CO)_2Cl_2$, $CpFe(CO)_2{}^{13}CH_3$, $Fe_3(CO)_{12}$, $Ru_3(CO)_{12}$, and $KFe_2Mn(CO)_{12}$ with a number of surfaces (including MgO, SiO_2, and C) have been studied. The chemistry of metal carbonyls in zeolite cages, as well as the nature of the

List of General Abbreviations on back endpaper

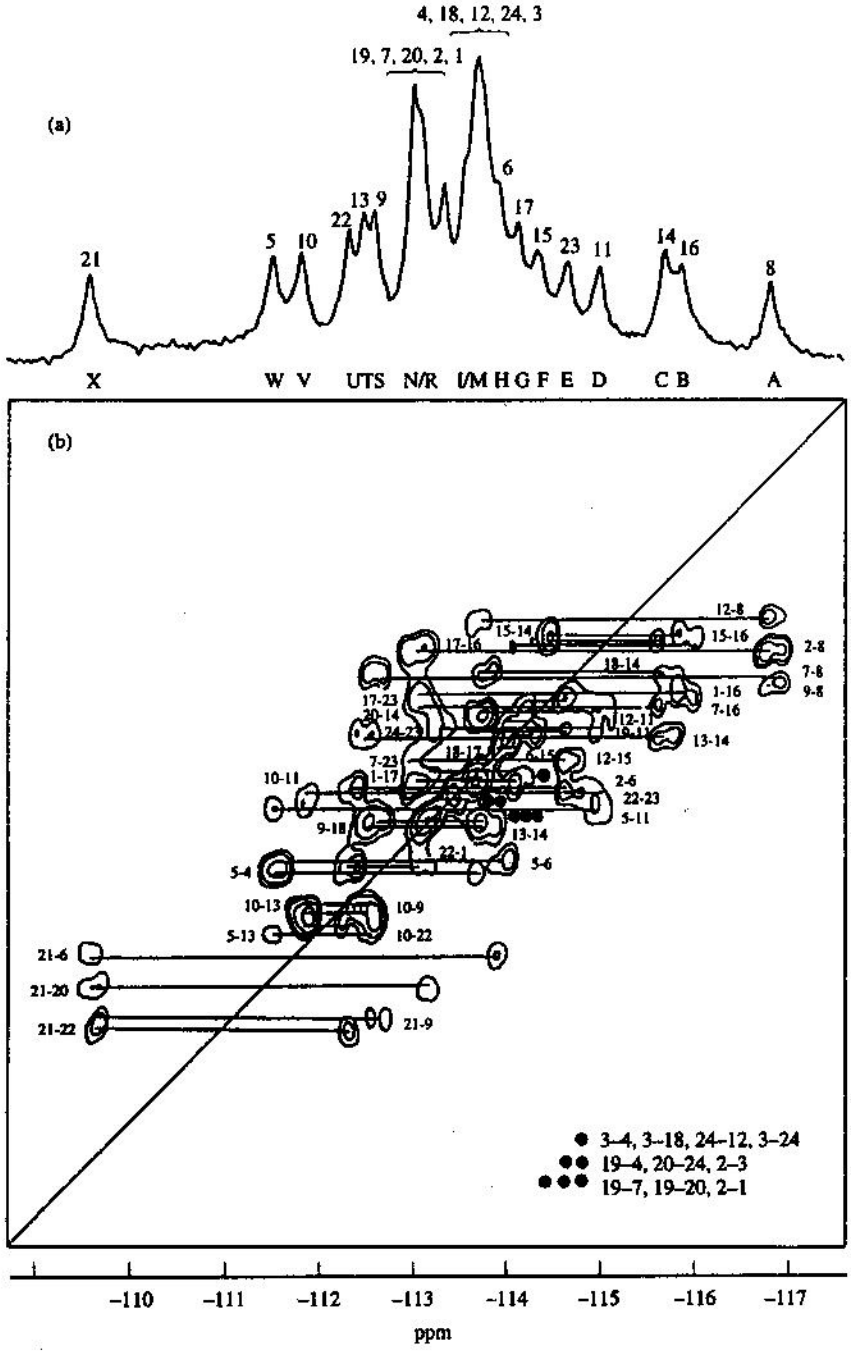

Figure 9 Silicon-29 MAS NMR spectra of ^{29}Si-enriched zeolite ZSM-5 at 300 K: (a) 1D spectrum; (b) 2D INADEQUATE experiment. (Reproduced by permission of Elsevier from Fyfe et al.[62])

interactions of metal alkenes, such as $Mo_2(C_3H_5)_4$ and $Zr(C_3H_5)_4$, with metal oxides have been reported, and ^{13}C MAS NMR has been shown to be capable of providing unique insights into adsorbate structure.[70–72]

Carbon-13 NMR has also been a useful method with which to investigate the direct interaction of small molecules, such as CO and C_2H_4, with supported metal catalysts (see ***Heterogeneous Catalysis by Metals***), e.g. CO on Rh/Al_2O_3, Pt/γ-Al_2O_3,[73] or C_2H_4 on Ag/α-Al_2O_3. It has been possible to determine, for example, C–O bond lengths for CO on Pt/γ-Al_2O_3, to detect bridge and end-bonded CO on Rh/γ-Al_2O_3, as well as identify 'bare' carbide-type carbon signals and study surface 'phase transitions'.[73] Many more applications of ^{13}C NMR in heterogeneous catalysis can be expected in the future.

For References see p.2658

3.3 Proton and Fluorine NMR

^{1}H and ^{19}F NMR have very high basic sensitivities, but strong homonuclear dipolar interactions cause considerable line broadening and loss of resolution. An interesting exception is when the nucleus is dilute, e.g. relatively isolated H_2O molecules in minerals, or in the case of the unusual symmetry arrangement of a linear arrangement of spins, such as the ^{19}F spins in fluorapatite ($Ca_5(PO_4)_3F$).[60] In both cases the homonuclear dipolar interaction is 'inhomogeneous', and slow MAS gives an envelope of sharp spinning sidebands, from which δ_{iso} can be measured. Obviously, these are special cases, and the general rule is that multiple pulse line narrowing[12,13] and/or very fast MAS are required for abundant ^{1}H, ^{19}F spin systems.

Use of very fast (~15 kHz) MAS has led to measurement of many ^{19}F chemical shifts, even in phases having high ^{19}F levels, e.g. SrF_2 (78.9 ppm), Hg_2F_2 (67.2 ppm), CaF_2 (58.2 ppm), SnF_2 (52.6 ppm), KF (32.8 ppm), SnF_4 (16.1 ppm), CdF_2 (–29.1 ppm), MgF_2 (–31.8 ppm), HgF_2 (–33.4 ppm), and NaF (–58 ppm), where the chemical shifts are in ppm from a C_6F_6 reference.[60] ^{19}F chemical shifts in these materials have not yet been analyzed in detail theoretically, but even a qualitative analysis permits study of topics such as fluoridation (the mineralization and demineralization of tooth enamel). Typical results for ^{19}F MAS NMR of CaF_2 (homogeneous broadening) and fluorapatite (inhomogeneous broadening) are shown in Figure 10, where it can be seen that slow MAS (3.9 kHz) has very little effect on the CaF_2 NMR spectrum (Figure 10a), while the same relatively slow spinning speed gives rise to a full manifold of sidebands in fluorapatite (Figure 10b),[60] due to the inhomogeneous dipolar broadening in the latter case.

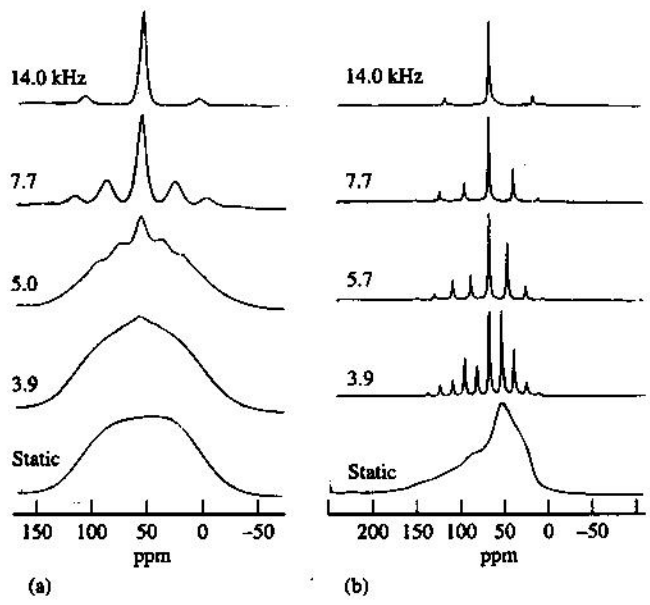

Figure 10 Fluorine-19 static and MAS NMR spectra of CaF_2 and fluorapatite ($Ca_5(PO_4)_3F$) at 7 T: (a) CaF_2; (b) fluorapatite. (Reproduced by permission of Academic Press from Kreinbrink et al.[60])

For ^{1}H systems in which homonuclear dipolar interactions are weak (because of structural or isotopic dilution), conventional MAS has been shown to be capable of giving important structural insights. A good example is the case of ZSM-5 catalysts in which the Al–(OH)–Si acid catalyst sites can be directly observed using ^{1}H MAS NMR methods. Here, the Al–O–H dipolar interactions can be determined, leading to an accurate structural model for the acid site. In addition, the actual ^{1}H chemical shifts give important information on the acidity of a given site (e.g. SiOH, Al(OH)Si, B(OH)Si).[74]

3.4 Other $I = \frac{1}{2}$ Systems

Most other common $I = \frac{1}{2}$ nuclei, such as ^{15}N, ^{31}P, ^{77}Se, ^{89}Y, ^{109}Ag, ^{113}Cd, ^{119}Sn, ^{125}Te, ^{183}W, ^{195}Pt, ^{199}Hg, ^{205}Tl, and ^{207}Pb, have been investigated in one or more inorganic solids, and the techniques used to obtain high-resolution spectra of these nuclei are basically the same as for the other dilute spin systems (^{13}C and ^{29}Si), i.e. magic angle sample spinning, with cross polarization where applicable. Since the chemistries of the different elements are so dissimilar, there is no underlying structural theme as found for Si, Al, and O. For example, ^{113}Cd studies have been reported in systems as diverse as semiconductors and proteins, while the subjects of phosphorus NMR studies range from ceramics and glasses again to semiconductors and novel porous framework $AlPO_{4-n}$ type materials. As with ^{29}Si NMR, two-dimensional methods, e.g. correlating ^{31}P and ^{113}Cd chemical shifts, or ^{31}P and ^{27}Al shifts,[54] are now appearing, and for very complex systems, two- and even three-dimensional methods will become even more important in the very near future.

4 RELATED ARTICLES

Borates: Solid State Chemistry; Carbonyl Complexes of the Transition Metals; Coordination Numbers & Geometries; Heterogeneous Catalysis by Metals; NMR in Inorganic Chemistry; Zeolites.

5 REFERENCES

1. E. Oldfield and R. J. Kirkpatrick, *Science*, 1985, **227**, 1537.
2. E. R. Andrew, A. Bradbury, and R. G. Eades, *Nature (London)*, 1959, **183**, 1802.
3. E. R. Andrew, in 'Progress in Nuclear Magnetic Resonance Spectroscopy', eds. J. W. Emsley, J. Feeney, and L. H. Sutcliffe, Pergamon, New York, 1971.
4. E. R. Andrew, W. S. Hinshaw, and R. S. Tiffen, *J. Magn. Reson.*, 1974, **15**, 191.
5. E. T. Lippmaa, M. A. Alla, T. J. Pehk, and G. Engelhardt, *J. Am. Chem. Soc.*, 1978, **100**, 1929.
6. D. Freude and H. J. Behrens, *Cryst. Res. Technol.*, 1981, **16**, K36.
7. D. Muller, W. Gessner, H. J. Behrens, and G. Scheler, *Chem. Phys. Lett.*, 1981, **79**, 59.

List of General Abbreviations on back endpaper

8. E. Kundla, A. Samoson, and E. Lippmaa, *Chem. Phys. Lett.*, 1981, **83**, 229.
9. E. Oldfield, S. Schramm, M. D. Meadows, K. A. Smith, R. A. Kinsey, and J. Ackerman, *J. Am. Chem. Soc.*, 1982, **104**, 919.
10. S. Schramm and E. Oldfield, *J. Chem. Soc., Chem. Commun.*, 1982, **77**, 4360.
11. M. D. Meadows, K. A. Smith, R. A. Kinsey, T. M. Rothgeb, R. P. Skarjune, and E. Oldfield, *Proc. Natl. Acad. Sci. USA*, 1982, **79**, 1351.
12. C. A. Fyfe, 'Solid State NMR for Chemists', CFC Press, Guelph, 1983.
13. G. Engelhardt and D. Michel, 'High Resolution Solid State NMR of Silicates and Zeolites', Wiley, New York, 1987.
14. A. Nolle, *Z. Phys. A*, 1977, **280**, 231.
15. S. Ganapathy, S. Schramm, and E. Oldfield, *J. Chem. Phys.*, 1982, **77**, 4360.
16. A. Samoson, E. Lippmaa, and A. Pines, *Mol. Phys.*, 1988, **65**, 1013.
17. A. Llor and J. Virlet, *Chem. Phys. Lett.*, 1988, **152**, 248.
18. B. F. Chmelka, K. T. Mueller, A. Pines, J. Stebbins, Y. Wu, and J. W. Zwanziger, *Nature (London)*, 1989, **339**, 42.
19. K. T. Mueller, Y. Wu, B. F. Chmelka, J. Stebbins, and A. Pines, *J. Am. Chem. Soc.*, 1991, **113**, 32.
20. K. T. Mueller, J. H. Baltisberger, E. W. Wooten, and A. Pines, *J. Phys. Chem.*, 1992, **96**, 7001.
21. I. Farnan, P. J. Grandinetti, J. H. Baltisberger, J. F. Stebbins, U. Werner, M. A. Eastman, and A. Pines, *Nature (London)*, 1992, **358**, 31.
22. J. H. Baltisberger, S. L. Gann, E. W. Wooten, T. H. Chang, K. T. Mueller, and A. Pines, *J. Am. Chem. Soc.*, 1992, **114**, 7489.
23. S. Schramm, R. J. Kirkpatrick, and E. Oldfield, *J. Am. Chem. Soc.*, 1983, **105**, 2483.
24. S. Schramm and E. Oldfield, *J. Am. Chem. Soc.*, 1984, **106**, 2502.
25. H. K. C. Timken, S. E. Schramm, R. J. Kirkpatrick, and E. Oldfield, *J. Phys. Chem.*, 1986, **91**, 1054.
26. T. H. Walter, G. L. Turner, and E. Oldfield, *J. Magn. Reson.*, 1988, **76**, 106.
27. H. K. C. Timken, G. L. Turner, J.-P. Gilson, L. B. Welsh, and E. Oldfield, *J. Am. Chem. Soc.*, 1986, **108**, 7231.
28. E. Oldfield, C. Coretsopoulos, S. Yang, L. Reven, H. C. Lee, J. Shore, O. H. Han, E. Ramli, and D. Hinks, *Phys. Rev. B*, 1989, **40**, 6832.
29. J. Herzfeld and A. E. Berger, *J. Chem. Phys.*, 1980, **73**, 6021.
30. J. P. Kintzinger, in 'NMR Basic Principles and Progress', eds. P. Diehl, E. Fluck, and R. Kosfeld, Springer-Verlag, New York, 1982, Vol. 17, p. 1.
31. E. Oldfield, M. A. Keniry, S. Shinoda, S. Schramm, T. L. Brown, and H. S. Gutowsky, *J. Chem. Soc., Chem. Commun.*, 1985, 791.
32. J. T. Cheng, J. C. Edwards, and P. D. Ellis, *J. Phys. Chem.*, 1990, **94**, 553.
33. W. P. Power, R. E. Wasylishen, S. Mooibroek, B. A. Pettit, and W. Danchura, *J. Phys. Chem.*, 1990, **94**, 591.
34. E. Oldfield, H. C. Lee, C. Coretsopoulos, F. Adebodun, K. D. Park, S. Yang, J. Chung, and B. Phillips, *J. Am. Chem. Soc.*, 1991, **113**, 8680.
35. Y. H. Yun and P. J. Bray, *J. Non-Cryst. Solids*, 1978, **27**, 363.
36. P. J. Bray, F. Bucholtz, A. E. Geissberger, and I. A. Harris, *Nucl. Instrum. Methods*, 1982, **199**, 1.
37. J. Zhong and P. J. Bray, *J. Non-Cryst. Solids*, 1989, **111**, 67.
38. K. F. M. G. J. Scholle and W. S. Veeman, *Zeolites*, 1985, **5**, 118.
39. G. L. Turner, K. A. Smith, R. J. Kirkpatrick, and E. Oldfield, *J. Magn. Reson.*, 1986, **67**, 544.
40. B. C. Bunker, R. J. Kirkpatrick, R. K. Brow, G. L. Turner, and C. Nelson, *J. Am. Ceram. Soc.*, 1991, **74**, 1430.
41. R. J. Kirkpatrick, T. Aselage, B. L. Phillips, and B. Montez, in 'Boron-rich Solids', eds. D. Emin, T. L. Asdage, A. C. Switendick, D. Moronin, and C. L. Beckel, AIP Conference Proceedings, American Institute of Physics, New York, 1991, Vol. 231.
42. I. Solomon, *Phys. Rev.*, 1958, **110**, 61.
43. E. Oldfield, H. K. C. Timken, B. Montez, and R. Ramachandran, *Nature (London)*, 1985, **318**, 163.
44. D. B. Zax, A. Bielecki, A. Pines, and S. W. Sinton, *Nature (London)*, 1984, **312**, 351.
45. A. C. Kunwar, G. L. Turner, and E. Oldfield, *J. Magn. Reson.*, 1986, **69**, 124.
46. J. Haase and E. Oldfield, *J. Magn. Reson. Ser. A*, 1993, **101**, 30.
47. E. Fukushima and S. B. W. Roeder, 'Experimental Pulse NMR', Addison-Wesley, Reading, MA, 1981.
48. D. Fenzke, D. Freude, T. Fröhlich, and J. Haase, *Chem. Phys. Lett.*, 1984, **111**, 171.
49. J. Haase, K. D. Park, K. Guo, H. K. C. Timken, and E. Oldfield, *J. Phys. Chem.*, 1991, **95**, 6996.
50. A. Avogadro, F. Tabak, M. Corti, and F. Borsa, *Phys. Rev. B*, 1990, **41**, 6137.
51. C. H. Pennington and C. P. Slichter, in 'Physical Properties of High Temperature Superconductors', ed. D. M. Ginsberg, World Scientific, Teaneck, NJ, 1990, Vol. II.
52. A. Pines, M. G. Gibby, and J. S. Waugh, *J. Chem. Phys.*, 1972, **56**, 1776.
53. T. H. Walter and E. Oldfield, *J. Phys. Chem.*, 1989, **93**, 6744.
54. E. R. H. van Eck and W. S. Veeman, *J. Am. Chem. Soc.*, 1993, **115**, 1168.
55. H. J. Jakobsen, J. Skibsted, H. Bildsøe, and N. C. Nielsen, *J. Magn. Reson.*, 1989, **85**, 173.
56. J. Skibsted, N. C. Nielsen, H. Bildsøe, and H. J. Jakobsen, *Chem. Phys. Lett.*, 1992, **188**, 405.
57. A. P. M. Kentgens, J. J. M. Lemmens, F. M. M. Geurts, and W. S. Veeman, *J. Magn. Reson.*, 1987, **71**, 62.
58. S. Ghose and T. Tsang, *Am. Mineral.*, 1973, **58**, 748.
59. C. H. Pennington, D. J. Durand, D. B. Zax, C. P. Slichter, J. P. Rice, E. D. Bukowski, and D. M. Ginsberg, *Adv. Magn. Reson.*, 1989, **13**, 1.
60. A. T. Kreinbrink, C. D. Sazavsky, J. W Pyrz, D. G. A. Nelson, and R. S. Honkonen, *J. Magn. Reson.*, 1990, **88**, 267.
61. M. Magi, E. Lippmaa, A. Samoson, G. Engelhardt, and A.-R. Grimmer, *J. Phys. Chem.*, 1984, **88**, 1518.
62. C. A. Fyfe, H. Grondey, Y. Feng, and G. T. Kokotailo, *Chem. Phys. Lett.*, 1990, **173**, 211.
63. N. Janes and E. Oldfield, *J. Am. Chem. Soc.*, 1985, **107**, 6769.
64. J. V. Smith and C. S. Blackwell, *Nature (London)*, 1983, **303**, 223.
65. R. Dupree, D. Holland, and M. G. Mortuza, *Nature (London)*, 1987, **328**, 416.
66. T. M. Duncan, *J. Phys. Chem. Ref. Data*, 1987, **16**, 125.
67. B. E. Hanson, in 'Advances in Dynamic Stereochemistry', ed. M. Gielin, Freund, London, 1985.

68. B. E. Hanson, M. J. Sullivan and R. J. Davis, *J. Am. Chem. Soc.*, 1984, **106**, 251.

69. T. H. Walter, L. Reven, and E. Oldfield, *J. Phys. Chem.*, 1989, **93**, 1320.

70. T. J. Marks, *Acc. Chem. Res.*, 1992, **25**, 57.

71. T. H. Walter, G. R. Frauenhoff, J. R. Shapley, and E. Oldfield, *Inorg. Chem.*, 1991, **30**, 4732.

72. L. Reven and E. Oldfield, *Inorg. Chem.*, 1992, **31**, 243.

73. L. R. Becerra, C. P. Slichter, and J. H. Sinfelt, *J. Phys. Chem.*, 1993, **97**, 10.

74. D. Freude, J. Klinowski, and H. Hamden, *Chem. Phys. Lett.*, 1988, **149**, 355.

Acknowledgments

This work was supported by NIH HL-19481 and NSF DMR 89-20538.